Accepted manuscript doi:
10.1680/jgeot.17.p.140

Submitted: 28 May 2017

Published online in 'accepted manuscript' format: 20 June 2018

Manuscript title: Swelling behaviour of compacted Maryland clay under different boundary conditions

Authors: S. Yuan*, O. Buzzi*[†], X. Liu* and J. Vaunat[‡]

Affiliations: *Priority Research Centre for Geotechnical and Materials Modelling, The University of Newcastle, Callaghan, NSW 2308, Australia; [†]Key Laboratory of High-speed Railway Engineering of Ministry of Education, School of Civil Engineering, Southwest Jiaotong Univeristy, Chengdu 610031, China and [‡]Department of Geotechnical Engineering and Geo-Sciences (ETCG), Polytechnic University of Catalonia (UPC), Barcelona

Corresponding author: X. Liu, Priority Research Centre for Geotechnical and Materials Modelling, The University of Newcastle, Callaghan, NSW 2308, Australia.

E-mail: xianfeng.liu@swjtu.edu.cn

Accepted manuscript doi:
10.1680/jgeot.17.p.140

Abstract

This paper presents an experimental study on the swelling response of compacted Maryland clay specimens subjected to hydration under a range of boundary conditions. The research is multi-scale with swelling tests complemented by comprehensive mercury intrusion porosimetry analyses. The objective of the experimental program is to establish the locus of final swollen states (in terms of void ratio and swelling pressure) and assess its robustness by testing a range of boundary conditions or combinations thereof. Five initial soil conditions were tested and swelling was generated by flooding or incremental suction reduction via the osmotic technique. The paper shows that, for a given soil condition, there is no influence of the stress-volume path on the final swollen state. This observation was corroborated at the microscopic level by the mercury intrusion porosimetry. It was concluded that the effect of different stiffness can actually be analysed in terms of the maximum stress applied to the specimen. In particular, a clear correlation was identified between the macroscopic strains and the confinement applied during the test, regardless of the boundary conditions. Also, the conceptual model relating the water ratio and micro void ratio proposed by Romero *et al*. (2011) was found to prevail, regardless of the boundary conditions.

Keywords: expansive soils; swelling; microstructure; MIP; SEM; double-structure

Accepted manuscript doi:
10.1680/jgeot.17.p.140

1 Introduction

Expansive soils are notoriously problematic for civil infrastructure because of the significant volume change experienced upon wetting and drying and because of the development of swelling pressure that accompanies swelling. The issue of expansive soil-structure interaction has received significant attention in the context of road pavements and retaining walls (e.g. Nelson and Miller, 1992; Lytton, 1994; Thomas, 2008; Brown, 2013) and scholars have devised methods to account for the expansiveness of the soil. Researchers have also explored the possibility chemically stabilize reactive soils (Nelson and Miller, 1992; Estabragh *et al*., 2014) in order to suppress their expansiveness. Using reactive soils in road project is not only a matter of volume change and swelling pressure. Indeed, Widger and Fredlund (1979) have reported stability problems for road embankments made of swelling clays. In conclusion, all published studies clearly show that expansive soils are far from being ideal construction materials. However, recently in Australia, increasing financial and environmental constraints have incited designers and road authorities to consider incorporating marginal materials, such as expansive soils, in civil infrastructure. For example, a number of encapsulated or zoned embankments have been designed and built on the Hunter Expressway, New South Wales (Aryal *et al*., 2012; Buzzi *et al*., 2012; Walter *et al*., 2012). The rationale of encapsulation is to prevent moisture uptake and offer some overburden pressure to counteract the swelling pressure. Achieving a satisfactory design requires a good understanding of the swelling behaviour of soils and, in particular, an adequate characterization of the swelling response under different boundary conditions. Much research has been conducted on swelling soils, especially under free swell and constant volume conditions (e.g. Yevnin and Zaslavsky, 1970; Kassiff and Ben Shalom, 1971; Brackley, 1973; Escario and Saez, 1973; Lloret and Villar,

2007; Cui *et al*., 2008, to name a few). In contrast, there is not much data on swelling under constant stiffness or under a combination of boundary conditions. Yet, such data are relevant for engineering applications where several boundary conditions are possible (see Siemens and Blatz, 2009; Lim and Siemens, 2016), which will possibly influence the relative proportion of swelling strain and swelling pressure being developed. Such idea was recently captured by Siemens and Blatz (2009) and Lim and Siemens (2016) via the concept of the Swelling Equilibrium Limit, noted SEL, which represents the locus of final swollen states. Although they did establish the SEL, the authors did not test its robustness by combining boundary conditions, nor did they account for the influence of the initial void ratio and suction. Lim and Siemens concluded that the SEL is a state line and, as such, it is not stress-volume path dependent. Although such results were corroborated by Liu *et al*. (2014), they are largely in contradiction with the general view that swelling is a stress path dependent phenomenon. For example, Nelson and Chao (2014) showed that a path where the soil swells under load followed by a recompression yields higher swelling pressures than if the soil swells under constant volume. Alonso *et al*. (2014) also provided experimental evidence of the stress path dependence of swelling pressure. Justo *et al*. (1984) reached the same conclusion for the magnitude of volume change.

Since the emergence of microstructural investigations in soil mechanics in the 1970s (Diamond, 1970; Sridharan *et al*., 1971), there is ample experimental evidence of the influence of the swelling condition on the evolution of the soil microstructure (Monroy *et al*., 2010; Romero *et al*., 2011; Yuan *et al*., 2016). However, as far as we know, there was no attempt to assess whether different stress-volume paths leading to the same overall swelling response could generate different microstructural changes. This paper presents a comprehensive multi scale study of the swelling response of compacted Maryland clay

specimens under a constant stiffness, constant volume, free swell, constant vertical stress and combination thereof. The objective of the study is to establish the locus of final swollen state (noted LFS here) for five different initial soil conditions, to assess its robustness and to check whether the locus is stress-volume path dependent. The study is strengthened by micro structural investigations that aim at assessing the effect of the stress-volume path on the extent of micro structural modifications undergone during swelling.

2 Experimental program and methods

2.1 Material and specimen preparation

The soil used in this study, Maryland clay, comes from the experimental field site of the University of Newcastle located in Maryland (NSW, Australia) established by Fityus *et al*. (2004). The mineralogical composition (provided in Table 1) shows that the soil contains about 10% of interlayered illite-smectite clay that confers to the soil a high reactivity. More details on Maryland clay can be found in Fityus and Smith (2004) and Liu *et al*. (2016).

This study focuses on compacted soil and the specimen preparation is consistent with that used in Liu *et al*. (2016) and Yuan *et al*. (2016): crumbs of natural soil were first dried in an oven at 105 °C, crushed to particles passing the 1.18 mm sieve and large organic matter (e.g. roots) were removed. The soil powder was wetted to three different water contents (13.2% 17.8% and 21.4%) using a water spray and the mixture was subsequently sealed in an air-tight plastic bag for two weeks for moisture equilibration.

Specimens of 45 mm diameter and 19 mm in height were prepared by static compaction in a loading frame. Void ratios of about 0.62 and 0.82 were targeted. Soil suction was also measured post compaction and after rebound using high capacity tensiometers (Mendes and

Accepted manuscript doi:
10.1680/jgeot.17.p.140

Buzzi, 2013) or a WP4 potentiameter (Decagon) in order to establish the wetting branch of the soil water retention curve (see Figure 1).

Mercury intrusion porosimetry analyses conducted after compaction showed in a bi-modal distribution of pores for all initial conditions tested here (further details on the method are given in section 2.3).

2.2 Apparatus for swelling under different boundary conditions

All tests were conducted using the swelling cell presented by Liu *et al*. (2014), which was upgraded to incorporate the capability to control suction via the osmotic method (Figure 3). The cell allows the application of a range of boundary conditions during swelling, namely constant volume, constant stress and constant stiffness (via springs of different stiffness). A load cell and a LVDT were used to record the swelling pressure force and the vertical displacement. The suction control is achieved by the osmotic method where a solution of polyethylene glycol (PEG) is circulated, in closed loop and via a peristaltic pump, from a reservoir to the bottom of the cell. The specimen is separated from the PEG solution via a semi-permeable Polyethersulfon (PES) membrane and a stainless porous plate (thickness of 3mm and dominant pore size of 10 microns). The whole setup was placed in a constant temperature room (control at ±0.5°C). The suction applied to the specimen is related to the PEG molecular weight, temperature and PEG concentration, as detailed in Yuan *et al*. (2017). The last stage of swelling, i.e. reducing suction to zero, was achieved by replacing the PEG solution by deionised water. Using deionised water from the beginning of the test is referred to as a "flooding" test since suction is reduced directly from its initial value to zero without any intermediate and controlled increments.

Note that conventional oedometers were used for swelling tests under constant vertical stress and flooding by deionized water. For all tests, evaporation was avoided by using a plastic membrane on the top part of the cell and, when applicable, some paraffin oil in the reservoir containing the PEG solution.

2.3 Mercury intrusion porosimetry

Mercury intrusion porosimetry (MIP) was used to track the changes in pore size distribution of the specimens upon swelling. A Micromeritics AutoPore IV 9500 with a maximal pressure of 228 MPa (corresponding to an equivalent entrance pore diameter of about 6.5 nm) was used and all the specimens (maximum volume of 1 cm^3) were subjected to a freeze drying process to remove the water with minimal effects on the soil structure. For the "freeze" phase, samples were immersed into the liquid nitrogen pre-cooled by vacuum (temperature of -210 °C). Then the frozen samples were placed in a freeze-dryer (Christ ® ALPHA 1-2) for at least 48 hours to sublimate the amorphous ice. After this process, the samples were sealed in airtight plastic vials and stored in a desiccator.

2.4 Experimental program

In the first series of tests, swelling was achieved by flooding, i.e. no incremental reduction of suction was applied. As detailed in Table 2, different combinations of initial void ratio, initial suctions and boundary conditions were tested. Such tests were completed in about 7 days. The tests under constant volume (CV), free swell (FS) and constant stiffness (CK) were used to establish the locus of final swollen state (noted LFS in the void ratio – net stress plane), for each combination of initial void ratio and initial suction. For the free swell condition, a vertical stress of 6kPa was applied. Note that the LFS can be considered equivalent to the swelling equilibrium line, or SEL, defined by Siemens and Blatz (2009) in the "specific

volume – mean stress" space. However, for a matter of clarity and rigor, a different terminology is used because the LFS and SEL are not defined in the same plane. The first series of tests is noted E_LFS_F, for "establish LFS under flooding".

A second series of test was conducted to track the evolution of the LFS as suction is incrementally reduced using the osmotic technique (series noted E_LFS_I, I for incremental). As for the first test series, five different boundary conditions were considered: free swell, constant volume and three tests at constant stiffness (k=489 N/mm, 175 N/mm and 55 N/mm). Due to the relatively long time required for equilibration after each suction change (around 4 weeks), only one initial soil condition was tested, namely w_o = 13.2% (s_o = 6.29 MPa) and e_o = 0.62.

Then, swelling tests under constant net stress and mixed boundary conditions were used to ascertain whether the final swollen state under different boundary conditions would still fall on the LFS, despite different stress-volume paths (series noted T_LFS_F, T for testing, F for flooding). For the tests under free swell followed by constant volume, during the free swell condition, a nominal load of 6 kPa is applied to the specimen. When a target swelling deformation has been achieved, deformation is prevented and the load cell records the swelling pressure exerted by the specimen. Table 2 summarizes the experimental program.

The evolution of soil microstructure, from initial state to the swollen state (either final or after a suction increment), was tracked using MIP. Although only a selection of results will be presented in this paper, microstructural investigations were conducted for all tests. Because MIP analyses are destructive, parallel specimens were used for the E_LFS_I series. In other words, one specimen was used for each boundary condition and each suction change. Only one specimen was subjected to an incremental reduction in suction, from 6290 kPa to zero in five steps with an MIP at the end of the test (test referred to as "k175_sev_inc" in Table 2).

Accepted manuscript doi:
10.1680/jgeot.17.p.140

3 Results and discussion

3.1 General swelling response

Figure 4 shows the evolution of swelling strain (defined as change of specimen height over initial height) and swelling pressure during a swelling test with two different values of stiffness (55 N/mm and 489 N/mm). The specimen was prepared at s_o=6.29 MPa and e_o = 0.62 and suction as reduced to zero in one step, by flooding.

All tests were stopped after the stabilization of either swelling pressure or strain, which occurs after the end of primary swelling. Because of the constant stiffness condition, both swelling strain and pressure develop during the test and the higher the stiffness, the lower the swelling strain and the higher the pressure. Such result is consistent with other data of the literature showing a drop in swelling pressure as more swelling strain is permitted (e.g. Uppal and Palit, 1969; Wang *et al*., 2012). Note that a positive value of strain corresponds to overall swelling, measured at the end of the test while a negative strain reflects overall collapse or compression. Collapse can also be partial, still resulting in an overall positive strain. In such case, the overall positive strain, as measured at the end of the test is reported in the rest of this paper.

3.2 Establishing the locus of final swollen states (LFS)

3.2.1 Flooding swelling tests

Figure 5 shows, for each set of initial condition, the locus of final swollen states (LFS), determined from the results of swelling tests by flooding under different boundary conditions. The dashed and continuous lines correspond to an initial void ratio of 0.82 and 0.62, respectively. Three different symbols are used to indicate the initial suction (empty circle: high suction (~6 MPa), full circle: low suction (0.8 MPa), half-full circle: mid suction (3

MPa). Consistent with other results of the literature (e.g. Uppal and Palit, 1969; Siemens and Blatz, 2009; Lim and Siemens, 2016), the swelling pressure reaches its maximum value under fully constrained condition and drops as less and less confinement is applied. The LFS shifts towards higher values of void ratio change and pressure as the initial void ratio decreases or/and the initial suction increases, which is not surprising considering that both these parameters are known to influence the magnitude of swelling. The locus of final swollen state (LFS) is established for a given set of initial conditions.

3.2.2 Incremental swelling tests

Figure 6 presents the development of swelling pressure and void ratio as suction is progressively reduced. Note that, the existence of a small void ratio change under constant volume condition is due to the deformability of the system. The progressive development of void ratio and pressure is consistent with the general knowledge of swelling behaviour: the higher the confinement exerted on the soil, the smaller void ratio change and the higher the swelling pressure. Figure 6a also shows that a large proportion of the total void ratio change develops at the low end of suction, as per experimental results of Escario and Saez (1973) and Kassiff *et al*. (1973).

The last suction reduction under constant volume was accompanied by some collapse with a final swelling pressure of 292 kPa, against 318 kPa at the previous step. This is the only occurrence of collapse observed for this series of tests.

Data of Figure 6 were transposed in the plane of the LFS in order to shows its progressive development (Figure 7). The LFS for suctions of ~4000kPa, ~2000kPa and ~1000kPa are non-monotonic but this is imputed to the experimental system (initial contact with the spring, stiffness of cell) rather than a soil response. Indeed, as shown in Figure 6, not much swelling takes place under such high suctions, which exacerbates the effect of experimental errors. For

values of suction lower than 1000kPa, the LFS is clearly defined and shifts upwards as the suction is reduced. The cross-over between LFS for suctions of 0 kPa and 100 kPa is due to the collapse observed in Figure 6. The void ratio-pressure path followed by the specimen that was subjected to several suction increments (k175_sev_inc, in Figure 7) is overall consistent with the other tests.

The water ratio e_w was calculated after each suction reduction increment and its evolution under different boundary conditions is showed in Figure 8. Note that, technically, these curves are not retention curves since the void ratio is not constant.

For suctions higher than about 350 kPa, the five curves are merged suggesting no effect of boundary conditions while at the low end of suction values, the curves diverge and the higher the stiffness, the lower the final water ratio. Such evolution is very similar to the retention at different void ratio where the void ratio only has an influence where capillary retention mechanism prevails (Romero et al., 1999). Figure 8 also includes some estimate of the degree of saturation of the macro pores (S_{rM}) using equation [1], which assumes that the micro pores are saturated:

$$S_{rM}=(e_w-e_m)/e_M \quad [1]$$

where e_M and e_m are the macro and micro void ratios, defined from the mercury intrusion curves using a micro-macro boundary of 1 micron (as per Yuan *et al*., 2016). Results suggest that the macro pores have reached a point of almost half saturation when the effect of boundary conditions becomes noticeable. In other words, although water is now located in the macro pores, where capillary retention mechanism is predominant, there is no noticeable effect of the boundary conditions and void ratio, which is surprising and not explained at this stage.

Accepted manuscript doi:
10.1680/jgeot.17.p.140

The evolution of microstructure for specimen along wetting path under different boundary condition is given in next section.

3.2.3 Microstructural changes during swelling

As discussed previously, several parallel specimens were used for the suction-control swelling tests in order to conduct microstructural analyses. Figure 9 show the pore size distribution for each boundary conditions and for three different values of suction (~1000kPa, ~100 kPa and ~0 kPa).

Reducing the suction from its initial value (6.29 MPa) to about 1 MPa is accompanied by microstructural changes that are largely unaffected by the nature of the boundary condition applied (Figure 9a). At this stage, the distribution is still bi-modal with dominant macro-pores of about 7 to 10 microns and dominant micro pores of about 0.05 microns.

Reducing the suction further (to about 0.1 MPa), lead to significant microstructural changes with a pore family appearing in between the two peaks that were present under 1MPa of suction (see Figure 9b). This corresponds to the onset of pore merging: the aggregates swell upon hydration, which leads to an increase in micro pore size and density. Concomitantly, the swelling aggregates can invade the inter-aggregate porosity (depending on the boundary condition applied), which translates into a reduction in macro pores size. Such observations are consistent with previous studies of the literature (Monroy *et al*., 2010; Romero *et al*., 2011; Yuan *et al*., 2016). Although the pore size distributions all largely remain bi-modal, an effect of the boundary condition now appears.

The most significant microstructural changes take place when suction is reduced from about 0.1 MPa to about 0 MPa (Figure 9c), which coincides with the large void ratio change visible in Figure 6a at the low end of suction. The pore size distributions now include only one dominant peak and the effect of the boundary condition is well pronounced: the free swell

condition leads to more of the larger pores while imposing a constant volume creates the opposite: smaller pores and lower density. The pore size distributions resulting from swelling under constant stiffness are very close, despite one order of magnitude between minimum and maximum stiffness, and are located in between the distributions associated with constant volume condition and free swell condition (see Figure 9c).

3.3 Influence of different stress-volume paths on final swollen state

One of the objectives of this study is to ascertain whether the final swollen state (i.e. final void ratio and final swelling pressure) depends on the stress-volume path followed during swelling for a given initial state of sample. The LFS was established with the first test series for each set of initial conditions (see Figure 5), and the swelling tests under constant vertical stress and mixed boundary conditions, represented by blue crosses and black lines in Figure 10, are here used to test the robustness of each LFS.

Clearly, for the five conditions tested, the stress-volume path followed does not significantly influence the final position on the LFS for a given set of initial conditions. Indeed, the majority of tests at constant vertical stress and mixed boundary conditions yield a combination of void ratio and swelling pressure in line for the LFS determined for each initial condition. Note that some collapse has occurred for the highest levels of stress applied. In conclusion, this series of tests suggest that, for the conditions tested, the LFS are not stress-volume path dependent. This finding complements the study by Siemens and Blatz (2009) and Lim and Siemens (2016) who tested different boundary conditions to establish the LFS but did not attempt to reach the same point of the LFS via different stress-volume paths.

Although the present results corroborate some previous studies (e.g. Siemens and Blatz, 2009; Lim and Siemens, 2016) they also contradict findings from other studies (e.g. Justo *et al*.,

1984; Alonso *et al*., 2013; Nelson and Chao, 2014; Alonso *et al*., 2014) that have concluded that both volume change and swelling pressure are stress path dependent.

7 points (A to G, details given in Table 3) were identified in Figure 10, for which two different stress-volume paths lead to very close final swollen states (i.e. pressure and void ratio). These points were chosen to assess whether soil specimens that fall close on the LFS share similar microstructural features.

The pore size distributions pertaining to points A, D, E and G are showed in Figure 11. Although the figure suggests that, for each point, following two different stress-volume paths may result in similar microstructure, this impression largely comes from the fact that there is little variability in the final pore size distributions.

For example, let us compare the pore size distribution of k55 in Figure 11a (point A) and that of CV in Figure 11b (point G): both are essentially mono-modal with a peak at about 1 micron and a density of about 0.5. Yet, the final swollen states of points A and G are very different (see Figure 10). Most importantly, points A and G correspond to specimens with different initial microstructure and the final microstructure on its own cannot reflect the extent of microstructural changes that take place during hydration.

It is here proposed to compare the initial and final mercury intrusion curves, and more precisely, to quantify the area located in between these intrusion curves. Such area can be considered a meaningful indicator of the magnitude of microstructural changes having taken place as a result of swelling. Figure 12a illustrates this concept for the initial condition e_o=0.82 and s_o=6.6 MPa.

The areas between intrusion curves, calculated for points A to G and for each boundary condition, are reported in Table 4. Figure 12b is a plot of points A to G, where their coordinates are the values reported Table 4. A point falling on the 1:1 line means that two

specimens having swollen to the same final state but under different boundary conditions have undergone the same magnitude of microstructural changes. For specimens having the same initial conditions, and hence, same initial microstructure, this further means that the specimens do have the same final microstructure. With points A to G falling very close to the 1:1 line, one can conclude that the almost-matching final swollen states appearing in Figure 10 is accompanied by almost-matching microstructural changes.

3.4 Influence of boundary conditions on microstructural changes

The change of micro void ratio (Δe_m) and macro void ratio (Δe_M) has been calculated from the evolution of pore size distribution. A boundary of 1 micron (consistent with Yuan et al., 2016) was used to identify the volumes of mercury intruded in micro pores and macro pores. These micro and macro volumes were then multiplied by the specific of the soil, which yields the micro and macro void ratios (as per Monroy *et al*., 2010; Romero *et al*., 2011). Figures 13a and 13b show that, for the two initial void ratios tested, the magnitude of confinement (applied stress or swelling pressure) clearly affects the expansion (positive Δe_M value) or collapse (negative Δe_M value) of the macro pores. This is in line with the conclusions drawn by Lloret and Villar (2007). There is no discernable influence of suction on the change of macro void ratio, except at the lowest end of stress, where significant swelling occurs. Interestingly, the nature of the boundary condition is not as significant as the magnitude of stress it will generate.

The micro void ratio was found to increase, for all boundary conditions applied, reflecting an expansion of the aggregates upon hydration. At a given suction, no clear correlation can be established between confinement applied (applied stress or swelling pressure) and change in micro void ratio. Again, this is in agreement with the observation by Lloret and Villar (2007), Monroy *et al*. (2010), Romero *et al*. (2011), Alonso *et al*. (2013), mechanical loading

generally affects the macro pores but only marginally impacts the micro pores. When it comes to suction, the trend seems inconsistent: although the highest initial suction results in the most swelling, the lowest one is not necessarily associated with the least swelling (see Figure 13c).

The incremental swelling tests offer the possibility to track the evolution of e_m during hydration (as a function of the water ratio, e_w). Results are presented in Figure 14 and interpreted in the light of the model proposed by Romero *et al.* (2011). The data is divided in two domains defined by a line of gradient equal to 1. Data on the left of the 1:1 line are considered to belong to the shrinkage limit domain where they are fitted using a horizontal line. In other words, no microscopic shrinkage occurs as the water ratio is reduced. Data on the right of the 1:1 line are fitted using the following equation:

$$e_m = e_m^* + \beta(e_w - e_m^*) \text{ for } e_w > e_m^* \quad [4]$$

where β quantifies the swelling tendency of aggregates and e_m^* is the boundary between the two domains. For $e_w > e_m^*$, the aggregates are considered fully saturated. The present data suggest that, for Maryland clay, β is equal to 0.3 and e_m^* is equal to 0.42, which is very close to the shrinkage limit of compacted Maryland clay reported in Buzzi *et al.* (2017). Interestingly, the evolution of e_m with e_w seems to be independent of the boundary conditions applied. Indeed, Figure 14 includes results of all five types of incremental swelling tests.

4 Concluding remarks

This paper presents a multi scale study of the swelling response of compacted Maryland clay specimens under a range of boundary conditions, including constant stiffness. The locus of final swollen (LFS) states, expressed in terms of void ratio and swelling pressure, was

established for five different initial conditions. Swelling tests with suction control by the osmotic technique were also conducted, in order to show the progressive development of the LFS, for one initial condition. The second series of tests showed that the final position of points on the LFS for a given set of initial conditions is not affected by the stress-volume path followed, which tends to confirm that the LFS can be considered as a state line, a concept proposed by Siemens and Blatz (2009) and Lim and Siemens (2016).

Microstructural investigations have complemented the swelling tests and brought some new insight into the swelling phenomenon. A number of publications have reported that an initially bi-modal pore size distribution can become mono-modal upon swelling. This study has now showed that such change occurs within the last stages of swelling (suction reduced from 100kPa to 0 kPa), where most of the volume change takes place.

The fact that the stress-volume path does not seem to affect the final position on the LFS was corroborated at the micro-scale, where similar microstructural changes upon swelling were recorded for specimens having swollen under different boundary conditions. Such conclusion could not be drawn from the analysis of only pore size distributions post swelling. The extent of microstructural changes was quantified by estimating the area between the intrusion curve before swelling and that after swelling. Finally, it was found that the type of boundary condition does not matter as much as the amount of confinement generated on the soil specimens. The confinement plays a key role on the evolution of macro void ratio upon swelling. In contrast, no clear trend could be highlighted between the change in micro void ratio, from initial to final states, and suction or confinement. Looking at the microstructural evolution during incremental swelling, the data (i.e. e_m and e_w) were found to follow a bi-linear trend, consistent with the conceptual model proposed by Romero *et al*. (2011), regardless of the boundary condition applied.

Accepted manuscript doi:
10.1680/jgeot.17.p.140

Acknowledgements

The authors would like to express their gratitude to the Australian Research Council (ARC) for the financial support (ARC DP110103304). The support from the China Scholarship Council (CSC) is also greatly acknowledged.

List of notations

S_{rM} degree of saturation of the macro pores

e_w water ratio

e_m micro void ratio

e_M macro void ratio

Δe_m change of micro void ratio

Δe_M change of macro void ratio

e_m^* critical water ratio that define the boundary of saturated and unsaturated micro void ratio

β swelling tendency of aggregates

Accepted manuscript doi:
10.1680/jgeot.17.p.140

References

Aryal S., Kingsland R., Och D., Sooklall A., Burton G., Russell G., and Buzzi O. (2012) Management of reactive and carbonaceous materials in the earthworks design for the Hunter Expressway, Minmi to Buchanan section. *The ANZ 2012 Conf. Proc., Melbourne*, 1304-1309.

Alonso, E.E., Pinyol, N.M., and Gens, A. (2013). Compacted soil behaviour: initial state, structure and constitutive modelling. *Géotechnique* 63, No. 6, 463–478.

Alonso E.E., Pinyol N., and Hoffman C. (2014). Highly Expansive granular mixtures. Unsaturated soils: research and applications. *Proc. 6th Int. Conf. Unsaturated Soils, Sydney*, 15-29.

Brackley I.J. (1973). Swell pressure and free swell in a compacted clay. *Proc. of the 3rd Int. Conf. Expansive Soils, Haifa, Israel*, 169–176.

Brown A.C. (2013). The Behavior of Drilled Shaft Retaining Walls in Expansive Clay Soils. PhD Thesis, the Univeristy of Texas at Austin.

Buzzi O., Fityus S., Kingsland R., and Aryal S. (2012) Monitoring of an encapsulated embankment for the validation of a dimensionless model for soil swelling. *The ANZ 2012 Conf. Proc., Melbourne*, 1075-1080.

Buzzi, O., Yuan, S., Liu, X., Romero, E., and Delage, P., (2017). On the definition of a boundary between micro- and macro-porosity for mercury intrusion porosimetry applied to clayey soil. *Géotechnique* submitted.

Cui, Y.J., Tang, A.M., Loiseau, C., and Delage, P. (2008). Determining the unsaturated hydraulic conductivity of a compacted sand-bentonite mixture under constant-volume and free-swell conditions. *Phys. Chem. Earth* 33, 462–471.

Diamond, S. (1970). Pore Size Distributions in Clays. *Clays Clay Miner*. 18, 7–23.

Escario, V., and Saez, J. (1973). Measurement of the properties of swelling and collapsing soils under controlled suction. *Proc. 3rd Int. Conf. Expansive Soils, Haifa, Israel*, 195-200.

Estabragh, A. R., Rafatjo, H., and Javadi, A. A. (2014). Treatment of an expansive soil by mechanical and chemical techniques. *Geosynthetics Int.* 21, No. 3, 233-243.

Fityus, S.G., and Smith, D.W. (2004). The development of a residual soil profile from a mudstone in a temperate climate. *Engng. Geol.* 74, No. 1, 39–56.

Fityus, S.G., Smith, D.W., and Allman, M.A. (2004). Expansive Soil Test Site Near Newcastle. *J. Geotech. Geoenviron. Engng* 130, No. 7, 686-695.

Justo, J.L., Delgado, A., and Ruiz, J. (1984). The influence of stress-path in the collapse-swelling of soils at the laboratory. *Proc. 5th Int. Conf. Expansive Soils, Adelaide*, 67–71.

Kassiff, G., and Ben Shalom, A. (1971). Experimental relationship between swell pressure and suction. *Géotechnique* 21,No. 3, 245–255.

Kassiff, G., Baker, R., and Ovadia, Y. (1973). Swell-pressure relationships at constant suction changes. *Proc. 3rd Int. Conf. Expansive Soils, Haifa, Israel*, 257-266.

Lim, B.F., and Siemens, G.A. (2016). Unifying Framework for Modeling Swelling Soil

Behaviour. *Can. Geotech. J*. 53, No. 9, 1495–1509.

Liu, X., Buzzi, O., and Vaunat, J. (2014). Influence of stress-volume path on swelling behavior of an expansive clay. *Proc. 6th Int. Conf. Unsat. Soils, Sydney*, 931-937.

Liu, X., Buzzi, O., Yuan, S., Mendes, J., and Fityus, S. (2016). Multi-scale characterization of the retention and shrinkage behaviour of four Australian clayey soils. *Can. Geotech. J.* 53, No. 5, 854-870.

Lloret, A., and Villar, M. V. (2007). Advances on the knowledge of the thermo-hydro-mechanical behaviour of heavily compacted "FEBEX" bentonite. *Phys. Chem. Earth* 32, No. 8, 701–715.

Lytton, R. L. (1994) Prediction of Movement in Expansive Clay. In Vertical and Horizontal Deformations of Foundations and Embankments, edited by Yeung, A. and Feaalio, G. Geotechnical Special Publication No. 40, ASCE, New York, 1827-1845.

Mendes, J., and Buzzi, O. (2013). New insight into cavitation mechanisms in high-capacity tensiometers based on high-speed photography. *Can. Geotech. J*. 50, No. 5, 550-556.

Monroy, R., Zdravkovic, L., and Ridley, A. (2010). Evolution of microstructure in compacted London clay during wetting and loading. *Géotechnique* 60, No. 2, 105–119.

Nelson, J.D, and Chao, K.C. (2014). Relationship between swelling pressures determined by constant volume and consolidation swell oedometer. *Proc. 6th Int. Conf. Unsaturated Soils, Sydney*, 891-896.

Nelson, J.D. and Miller, D.J. (1992). Expansive soils: problems and practice in foundation and pavement engineering. Wiley, New York.

Romero, E., Gens, A., and Lloret, A. (1999). Water permeability, water retention and microstructure of unsaturated Boom clay. *Engng. Geol.* 54, 117–127

Romero, E., Della Vecchia, G., and Jommi, C. (2011). An insight into the water retention properties of compacted clayey soils. *Géotechnique* 61, No. 4, 313–328.

Siemens, G., and Blatz, J.A. (2009). Evaluation of the influence of boundary confinement on the behaviour of unsaturated swelling clay soils. *Can. Geotech. J*. 46, No. 3, 339–356.

Sridharan A., Altschaeffl A.G., and Diamond S. (1971). Pore size distribution studies. *J. Soil Mech. Found. Div*. 97, SM5, 771–787

Thomas, M.G. (2008). Impact of lateral swell pressure on retaining structure design using expansive cohesive backfill. M. Sc. Thesis, The University of Texas at Arlington.

Uppal, H.L., and Palit, P.L. (1969). Measurement of swelling pressure of expansive soils. *Proc. 2nd Int. Res. Engng. Conf. Expansive Clay Soils, Texas*, 250-255.

Wang, Q., Tang, A.M., Cui, Y.J., Delage, P., and Gatmiri, B. (2012). Experimental study on the swelling behaviour of bentonite/claystone mixture. *Engng. Geol*. 124, No. 1, 59-66.

Walter P., Anwar S., and Sutherland M. (2012). Performance of pavements constructed with expansive clay. *Proc. 25th ARRB Conf., Perth, Australia*.

Widger R.A., and Fredlund D.G. (1979). Stability of swelling clay embankments. *Can. Geotech. J*., 16, No. 1, 140-151.

Yevnin, A., and Zaslavsky, D. (1970). Some factors affecting compacted clay swelling. *Can. Geotech. J.* 7, No. 1, 79–91.

Yuan, S., Liu, X., and Buzzi, O. (2017). Calibration of a coupled model to predict the suction generated by the osmotic technique with PES membranes and temperature effect. *Geotech. Test. J*. 40, No. 1, 144-147.

Yuan, S., Liu, X., Sloan, S.W., and Buzzi, O.P. (2016). Multi-scale characterization of swelling behaviour of compacted Maryland clay. *Acta Geotech*. 11, No. 4, 789–804.

Table 1 Physico-chemical properties of Maryland clay (modified from Liu *et al*., 2016)

Mineralogy composition by Quantitative XRD analysis (% in mass)	**Interlayered illite-smectite clay (10 %) Kaolinite (26 %), Quartz (36.9 %), Mica (17.4 %) K-feldspar (3.3 %), Plagioclase (5.8 %)**
Organic matter content (% in mass)	1.5
Specific gravity (Gs)	2.65
Atterberg limits (%)	Liquid limit (W_L): 69.8, Plastic limit (W_P): 24.1
Linear shrinkage potential (%)	14
Total surface area (m^2/g)	95.2
Total C.E.C (meq/100g)	14.0

Accepted manuscript doi:
10.1680/jgeot.17.p.140

Table 2: Summary of the experimental testing program.

Series Name	**Boundary conditions (and test names)**	**Combination of initial conditions tested**	
		e_o	w_o [%] (s_o [MPa])
E_LFS_F	Free Swell (noted FS) Constant volume (noted CV) Constant Stiffness (noted k# where # is the stiffness equal to 55, 175 or 489 N/mm	0.62	13.2 (6.29) 17.8 (3.04) 21.4 (0.80)
		0.82	13.2 (6.66) 17.8 (3.00)
E_LFS_I	CV, final suction [kPa]: 4165, 2076, 965, 635, 115, 0	0.62	13.2 (6.29)
	k489, final suction [kPa]: 4812, 2005, 1045, 122, 0		
	k175, final suction [kPa]: 4677, 2029, 991, 532, 206, 0		
	k175_sev_inc, suction increments [kPa]: 4588, 2350, 1087, 501, 206, 0		
	k55, final suction [kPa]: 4415, 2076, 494, 210, 0		
	FS, final suction [kPa]: 1960, 1045, 486, 224, 88, 0		
T_LFS_F	Constant vertical stress (noted CS# where # is the vertical stress equal to 50, 100, 200, 300 or 400 kPa	0.62	13.2 (6.29) 17.8 (3.04) 21.4 (0.80)
		0.82	13.2 (6.66) 17.8 (3.00)
	Free swell followed by Constant volume (FS+CV)	0.62	17.8 (3.04) 21.4 (0.80)
		0.82	13.2 (6.66)
	Swelling with 175 N/mm followed by Constant volume – (k55+CV)	0.62	17.8 (3.04)
		0.82	13.2 (6.66)

Accepted manuscript doi:
10.1680/jgeot.17.p.140

Table 3: Initial states and boundary conditions (BC) pertaining to points A and G of Figure 10.

Point	**A**	**B**	**C**	**D**	**E**	**F**	**G**
e_o	0.62	0.62	0.62	0.62	0.62	0.82	0.82
s_o [MPa]	6.29	3.00	3.00	0.80	0.80	6.66	3.00
BC 1	CS50	k175+CV	CS400	CS100	CS300	CS50	CS100
BC 2	k55	k489	CV	FS+CV	CV	k175	CV

Table 4 Magnitude of microstructural changes undergone during swelling and expressed as the area located between the intrusion curve of the as-compacted state and that of the final swollen state. For each point A – G (refer to Figure 10), two different boundary conditions are considered.

Point	**A**	**B**	**C**	**D**	**E**	**F**	**G**
Area 1 for BC1 [kPa]	36069	13146	7131	13621	5360	38804	15164
Area 2 for BC2 [kPa]	40554	14386	9687	11540	3131	31570	9577

Accepted manuscript doi:
10.1680/jgeot.17.p.140

Figure captions

Figure 1: Relationship between initial water content w_o and initial suction s_o, for compacted Maryland clay. Suction was measured post compaction using a high capacity tensiometer (for suctions below 1.5 MPa) and a WP4 potentiameter by Decagon (for suctions higher than 1.5 MPa).

Figure 2: Pore size distributions, obtained by mercury intrusion porosimetry, of specimens post compaction for three different initial suctions and two initial void ratios. (a): e_o=0.62, (b): e_o=0.82.

Figure 3: Sketch of the osmotic oedometer for swelling under different boundary condition.

Figure 4**:** Response of a specimen of Maryland clay compacted at e_o=0.62 and s_o=6.29 MPa and swelling by flooding under constant stiffness: (a) evolution of swelling pressure in time. (b) evolution of swelling strain in time. (c): relationship between swelling pressure (computed from recorded swelling force) and swelling strain (computed from measured vertical displacement) showing the constant stiffness. Suction was reduced from 6.29 MPa to 0 MPa.

Figure 5: Results of test series E_LFS_F: locus of final swollen states (LFS) in the "void ratio –swelling pressure" plan established for the five different initial conditions and using swelling tests under constant volume, free swell and constant stiffness.

Figure 6: Evolution of void ratio (a) and swelling pressure (b) as suction is progressively reduced to zero. Specimen was compacted at e_o =0.62, s_o=6.29MPa. Swelling tests were performed under five boundary conditions. Final suction is shown as 1kPa to avoid incompatibility with the logarithmic scale.

Figure 7: Results of test series E_LFS_I: combination of void ratio and swelling pressure for different values of imposed suction. Initial suction s_o =6.29 MPa, initial void ratio e_o = 0.62. The specimen undergoing several suction increments is represented in blue and labelled "k175_sev_inc".

Figure 8: Evolution of water ratio (e_w) as a function of suction (s) during incremental swelling under different boundary conditions.

Figure 9: Evolution of microstructure with different boundary conditions at constant applied suction: (a) $s_{applied}$= 1MPa; (b) $s_{applied}$= 0.1MPa; and (c) $s_{applied}$=0MPa.

Figure 10: Results of all swelling by flooding tests expressed in the "void ratio -swelling pressure" plane. (a), (b), (c) initial void ratio 0.62; (d), (e) initial void ratio 0.82. Test series E_LFS_F (empty circles) was used to establish the LFS while test series T_LFS_F (blue crosses and black line with diamond) was used to assess the robustness of the LFS.

Figure 11: Pore size distribution of soil specimens post swelling. (a): point A; (b): point G; (c): point E, (d): Point D. Test conditions are reported in Table 4.

Figure 12: (a) Mercury intrusion curves for specimen compacted at e_o=0.82 with s_o=6.6 MPa and after swelling under a stiffness of 489N/mm. The total area between the two intrusion curves is computed. (a) Plot of points A to G using coordinates (Area 1, Area 2) equal to the values reported in Table 4.

Accepted manuscript doi:
10.1680/jgeot.17.p.140

Figure 13: Change of macro and micro void ratios, from initial state to final swollen state, as a function of the swelling pressure developed by the sample for test series E_LFS_F and T_LFS_F. (a) Macro void ratio change (Δe_M) for e_o=0.62 and 3 different initial suctions; (b): Macro void ratio change (Δe_M) for e_o=0.82 and 2 different initial suctions; (c): Micro void ratio change (Δe_m) for e_o=0.62 and 3 different initial suctions; (d): Micro void ratio change (Δe_m) for e_o=0.82 and 2 different initial suctions.

Figure 14: Evolution of micro void ratio (e_m) with water ratio (e_w) for different boundary conditions for sample compacted at e_o=0.62 and s_o =6.29 MPa. The dashed line is a line of gradient 1. The red curve is a bi-linear best fit of the data of equation e_m=0.42+0.3×(e_w-0.42).

Accepted manuscript doi:
10.1680/jgeot.17.p.140

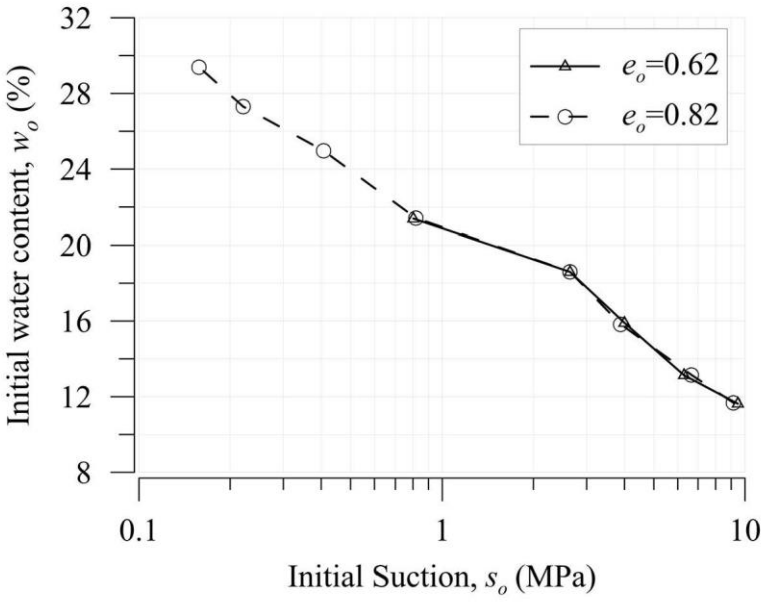

Fig01

Accepted manuscript doi:
10.1680/jgeot.17.p.140

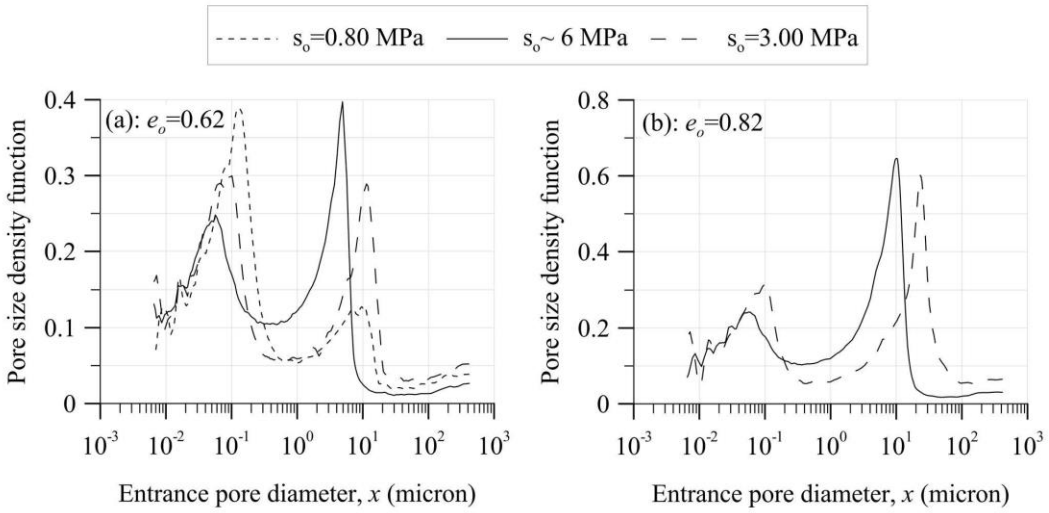

Fig02

Accepted manuscript doi:
10.1680/jgeot.17.p.140

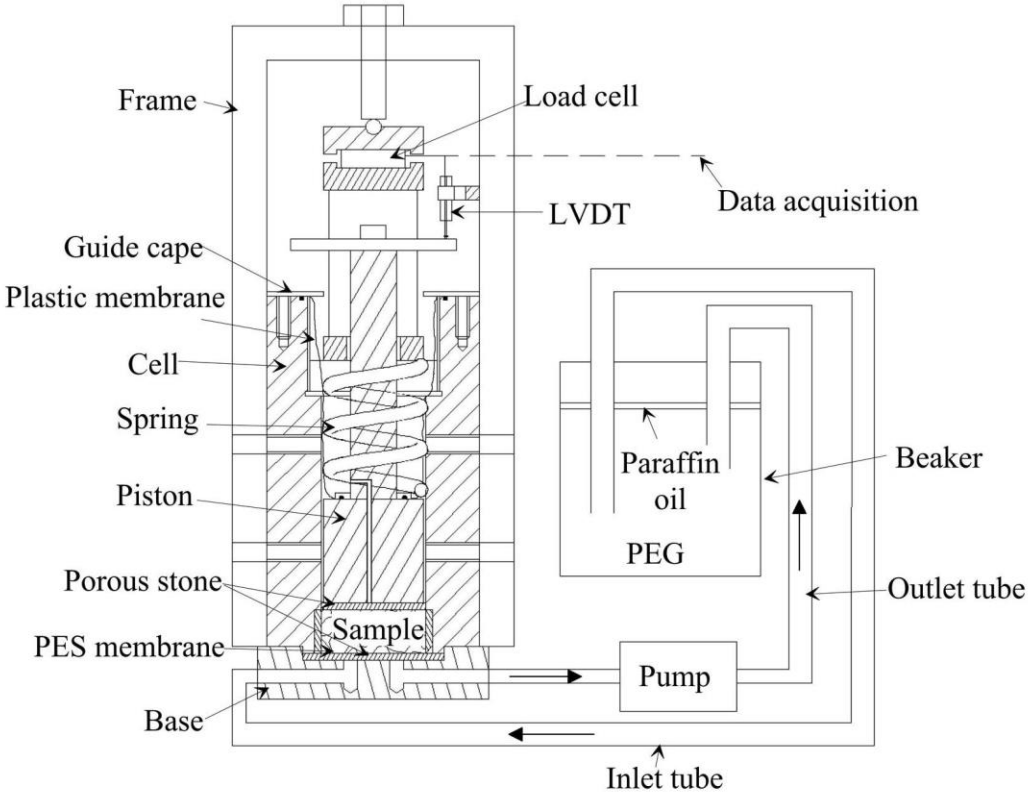

Fig03

Accepted manuscript doi:
10.1680/jgeot.17.p.140

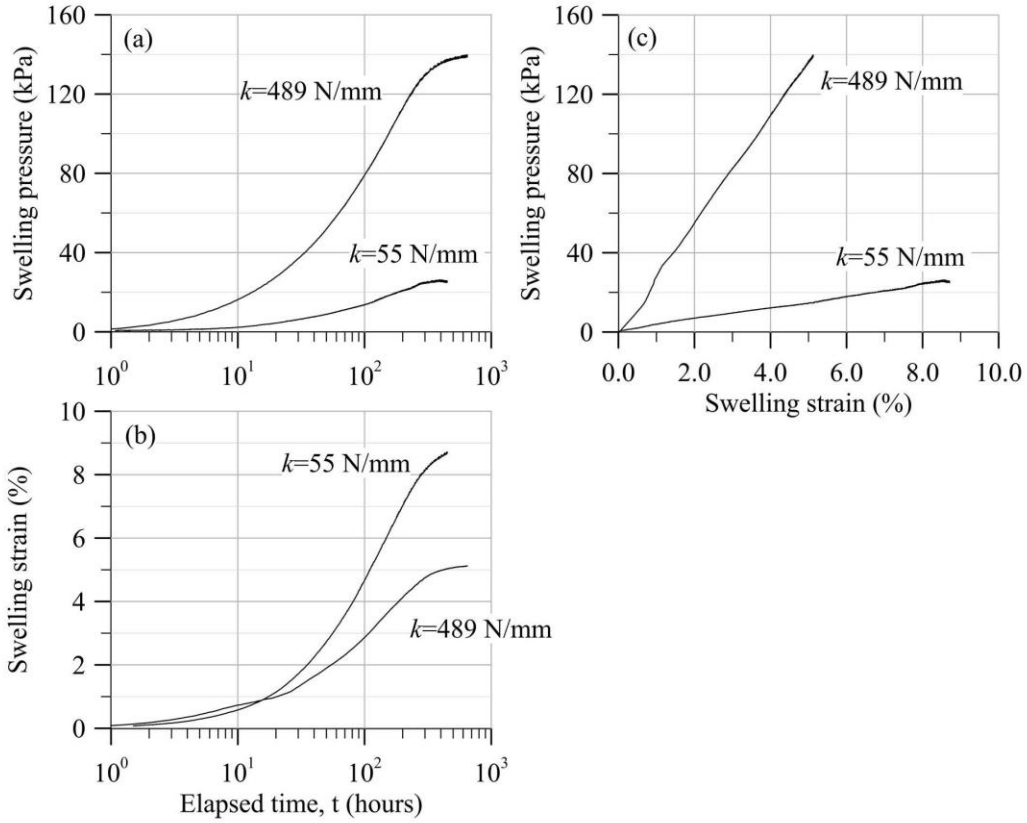

Fig04

Accepted manuscript doi:
10.1680/jgeot.17.p.140

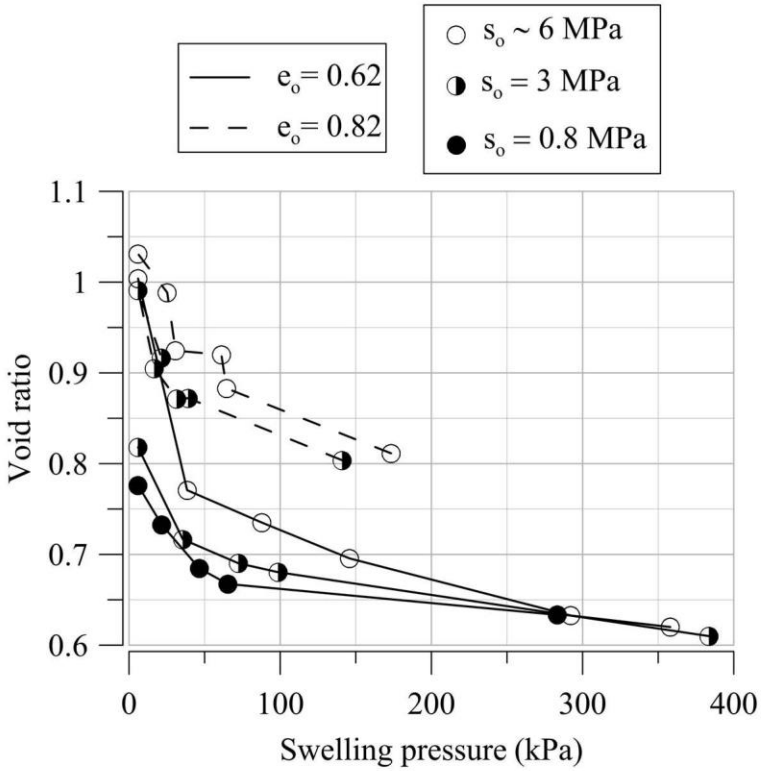

Fig05

Accepted manuscript doi:
10.1680/jgeot.17.p.140

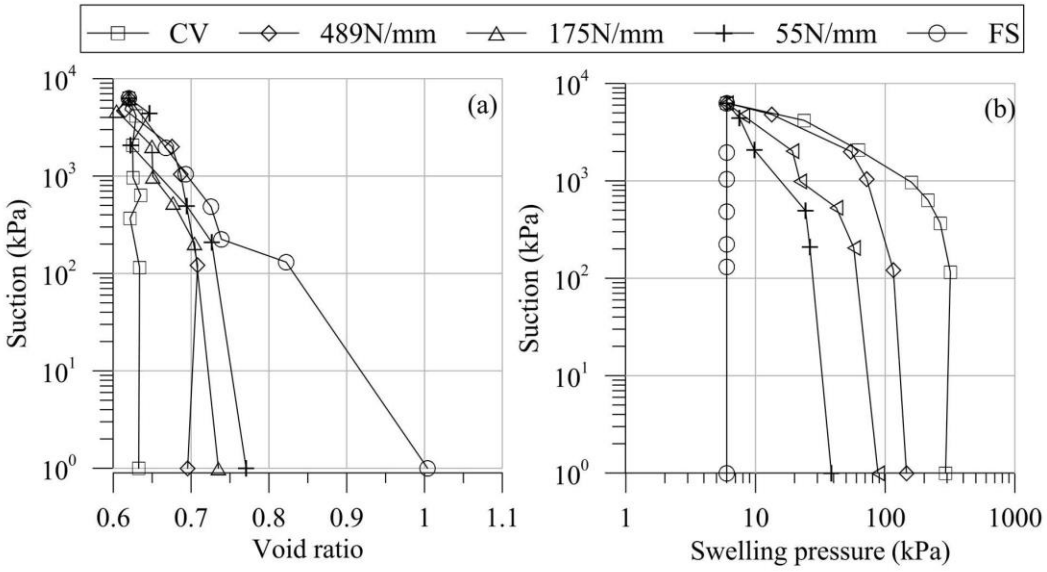

Fig06

Accepted manuscript doi:
10.1680/jgeot.17.p.140

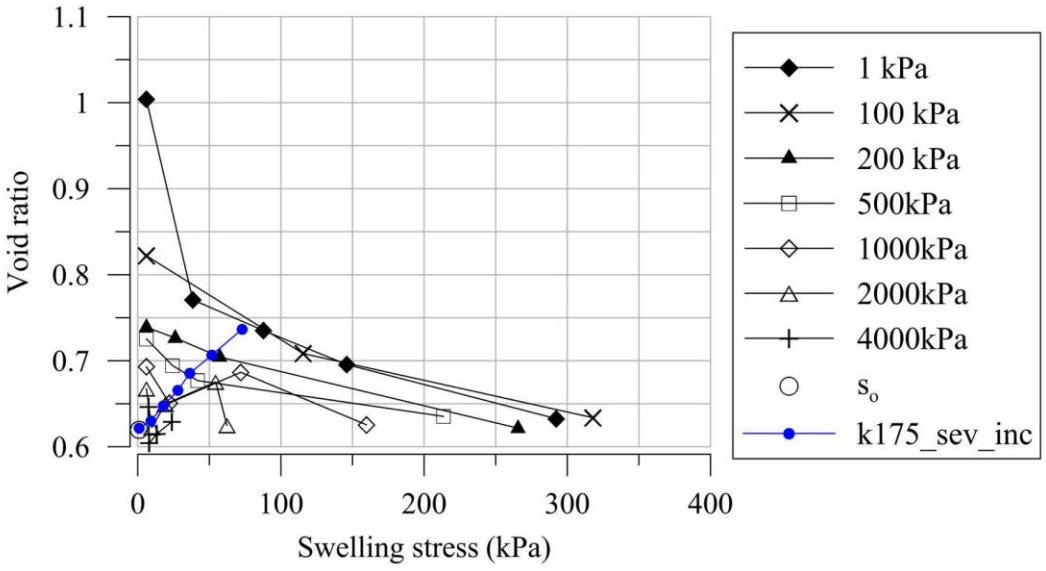

Fig07

Accepted manuscript doi:
10.1680/jgeot.17.p.140

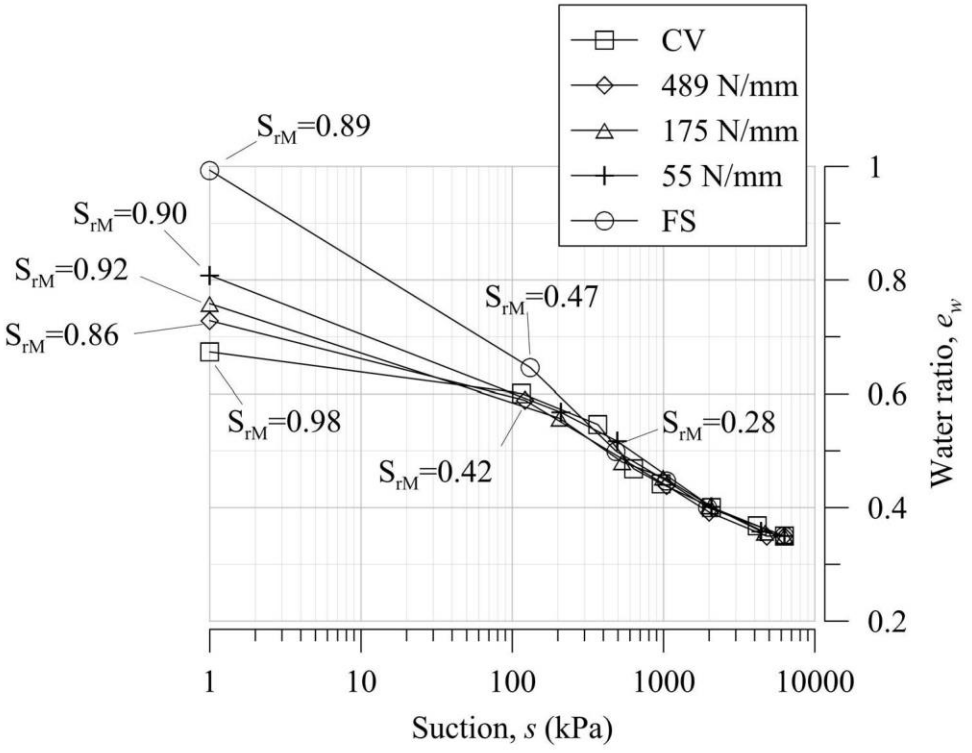

Fig08

Accepted manuscript doi:
10.1680/jgeot.17.p.140

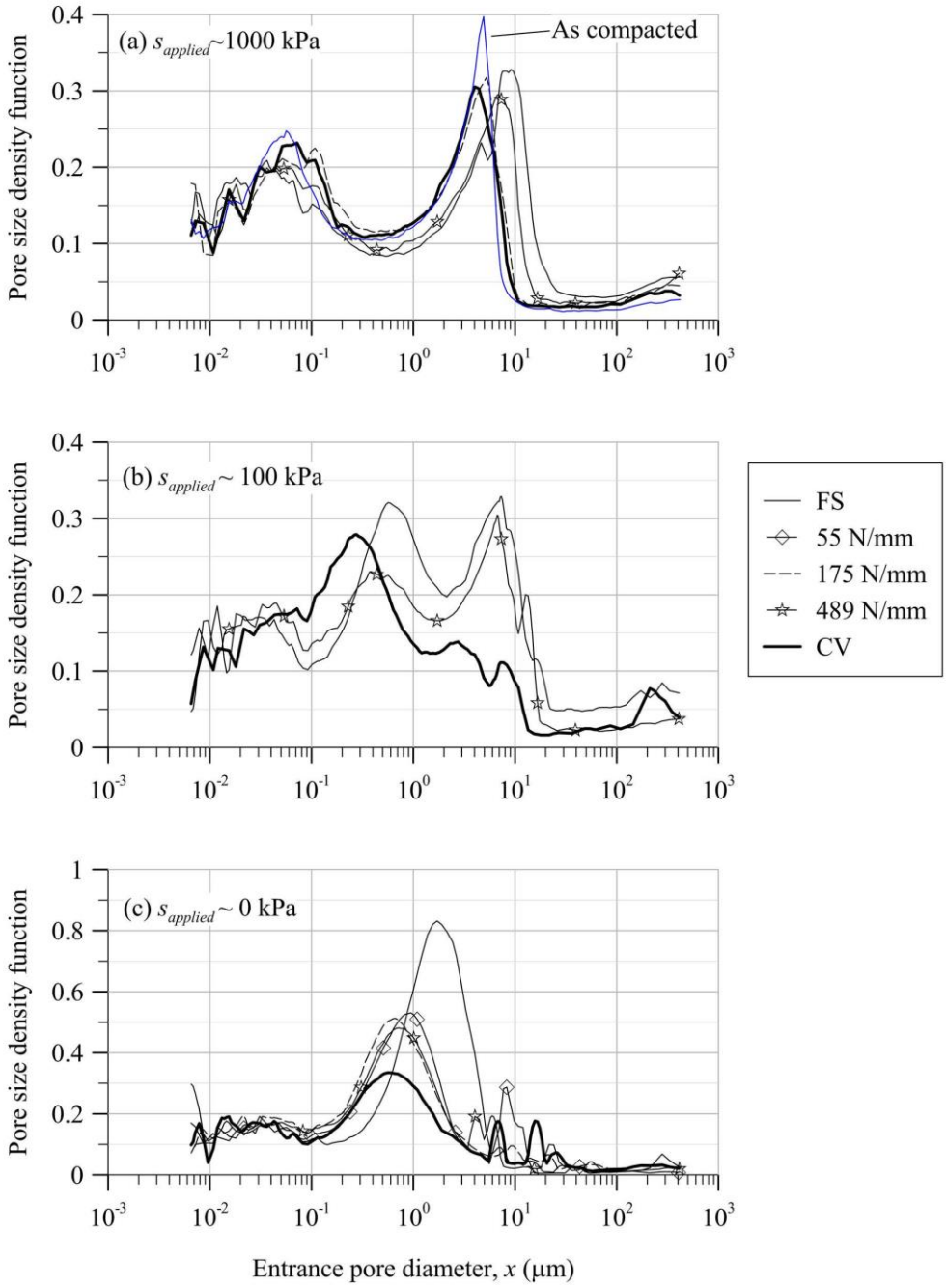

Fig09

Accepted manuscript doi:
10.1680/jgeot.17.p.140

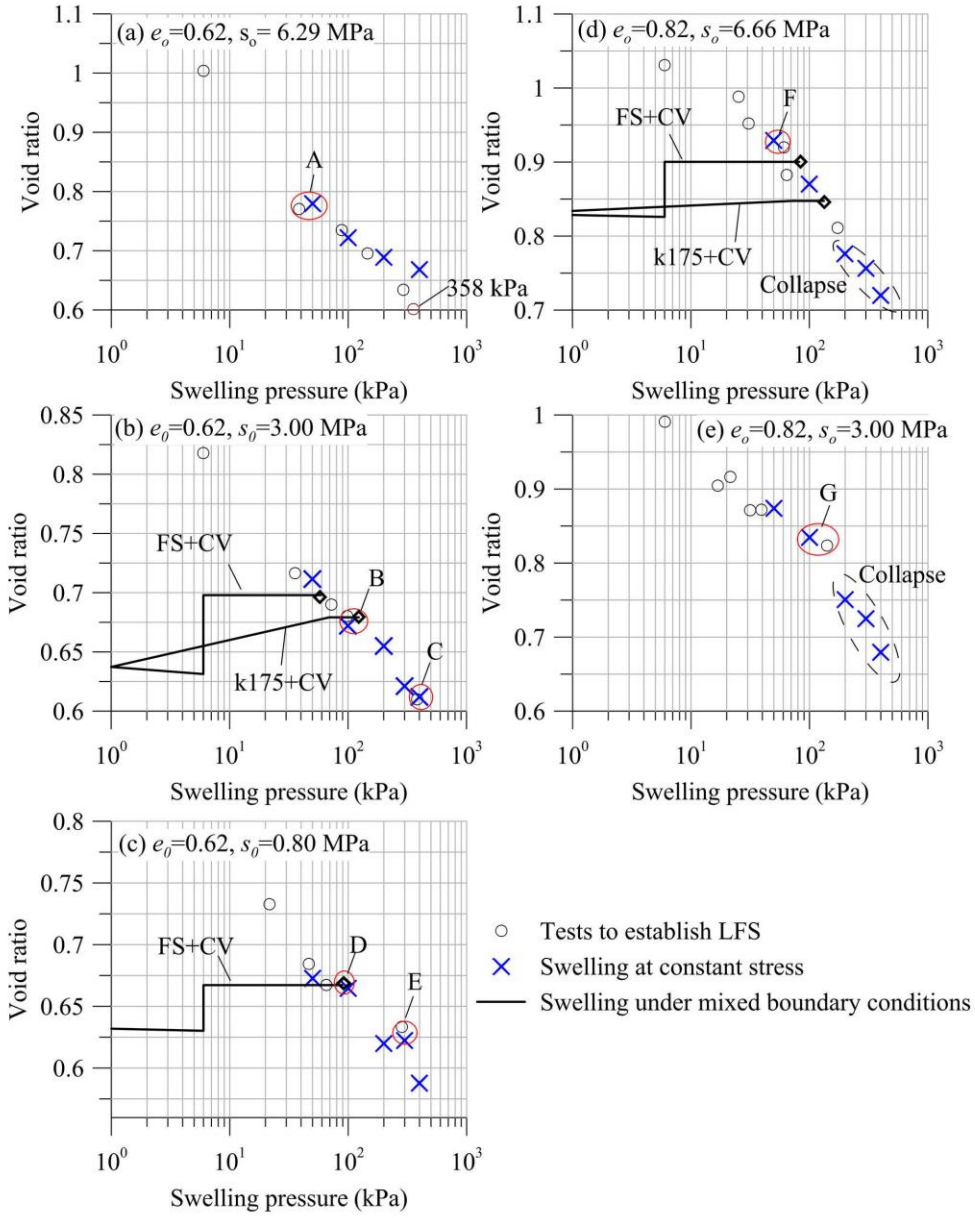

Fig10

Accepted manuscript doi:
10.1680/jgeot.17.p.140

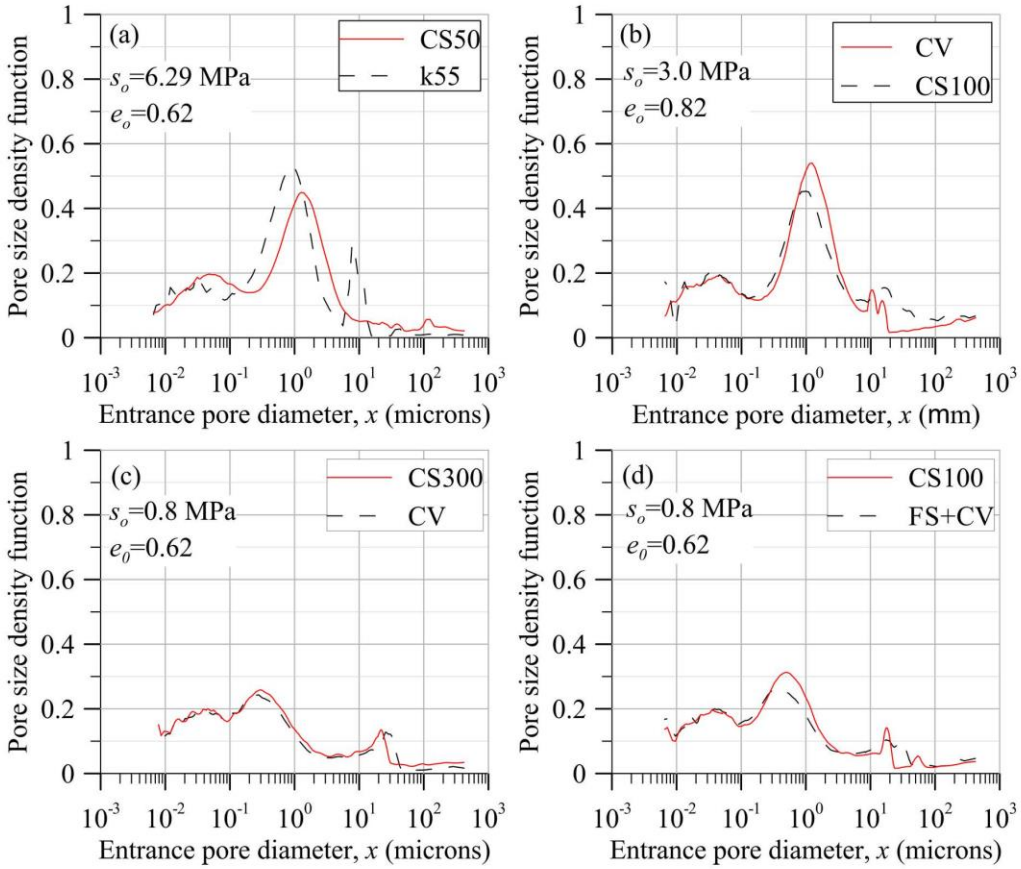

Fig11

Accepted manuscript doi:
10.1680/jgeot.17.p.140

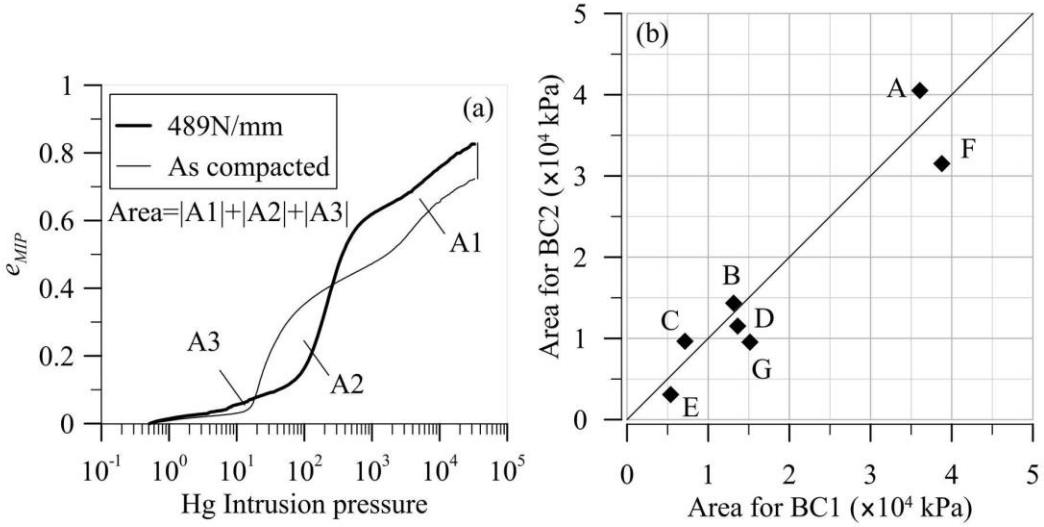

Fig12

Accepted manuscript doi:
10.1680/jgeot.17.p.140

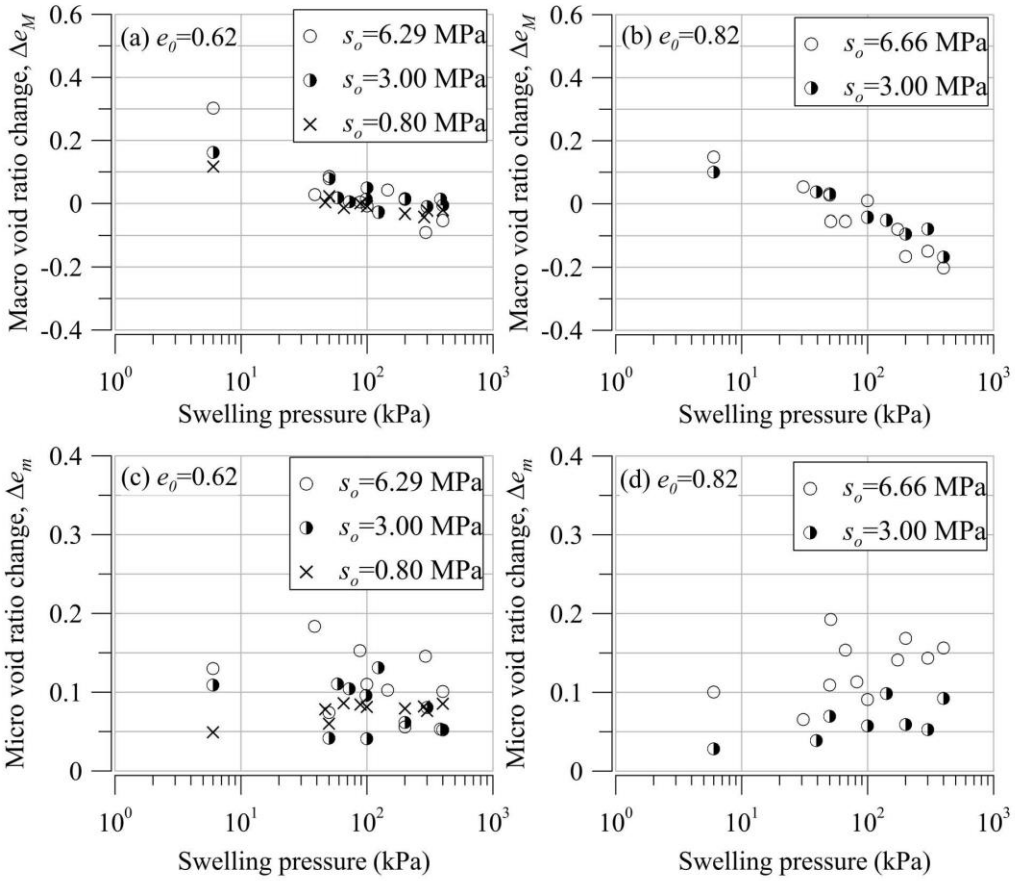

Fig13

Accepted manuscript doi:
10.1680/jgeot.17.p.140

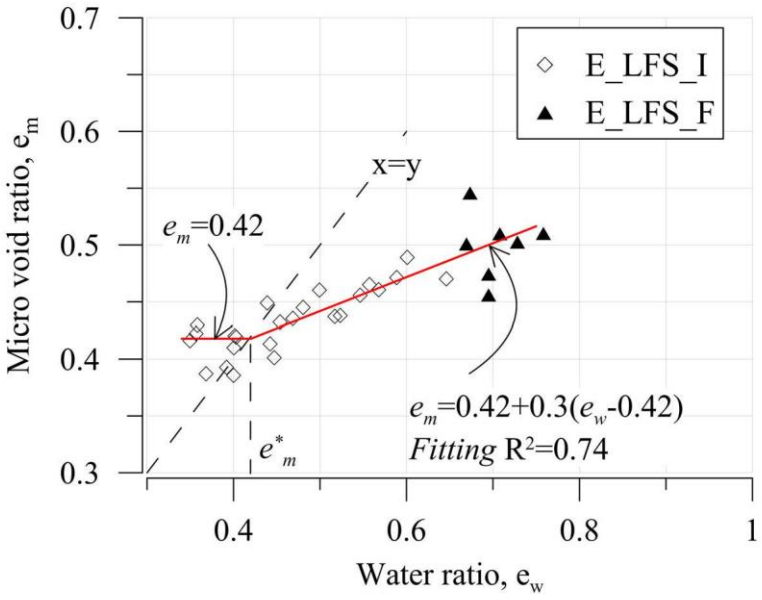

Fig14